On the Roles of Ca^{2+} Diffusion, Ca^{2+} Buffers, and the Endoplasmic Reticulum in IP_3-Induced Ca^{2+} Waves

M. Saleet Jafri* and Joel Keizer‡
*Institute of Theoretical Dynamics and ‡Institute of Theoretical Dynamics and Section on Neurobiology, Physiology, and Behavior
University of California, Davis, California 95616 USA

ABSTRACT We have investigated the effects of Ca^{2+} diffusion, mobile and stationary Ca^{2+} buffers in the cytosol, and Ca^{2+} handling by the endoplasmic reticulum on inositol 1,4,5-trisphosphate-induced Ca^{2+} wave propagation. Rapid equilibration of free and bound Ca^{2+} is used to describe Ca^{2+} sequestration by buffers in both the cytosol and endoplasmic reticulum (ER) lumen. Cytosolic Ca^{2+} regulation is based on a kinetic model of the inositol 1,4,5-trisphosphate (IP_3) receptor of De Young and Keizer that includes activation and inhibition of the IP_3 receptor Ca^{2+} channel in the ER membrane and SERCA Ca^{2+} pumps in the ER. Diffusion of Ca^{2+} in the cytosol and the ER and the breakdown and diffusion of IP_3 are also included in our calculations. Although Ca^{2+} diffusion is severely limited because of buffering, when conditions are chosen just below the threshold for Ca^{2+} oscillations, a pulse of IP_3 or Ca^{2+} results in a solitary trigger wave that requires diffusion of Ca^{2+} for its propagation. In the oscillatory regime repetitive wave trains are observed, but for this type of wave neither the wave shape nor the speed is strongly dependent on the diffusion of Ca^{2+}. Local phase differences lead to waves that are predominately kinematic in nature, so that the wave speed (c) is related to the wavelength (λ) and the period of the oscillations (τ) approximately by the formula $c = \lambda/\tau$. The period is determined by features that control the oscillations, including $[IP_3]$ and pump activity, which are related to recent experiments. Both solitary waves and wave trains are accompanied by a Ca^{2+} depletion wave in the ER lumen, similar to that observed in cortical preparations from sea urchin eggs. We explore the effect of endogenous and exogenous Ca^{2+} buffers on wave speed and wave shape, which can be explained in terms of three distinct effects of buffering, and show that exogenous buffers or Ca^{2+} dyes can have considerable influence on the amplitude and width of the waves.

INTRODUCTION

Calcium oscillations are seen in a variety of cells in response to stimulation by receptor-mediated agonist (Berridge, 1993). The binding of agonist to cell surface receptors results in the production of inositol 1,4,5-trisphosphate (IP_3) in the peripheral cytoplasm. The IP_3 diffuses rapidly into the cell interior, where it can bind to the IP_3 receptor/Ca^{2+} channel (IP_3R) in the endoplasmic reticulum (ER), activating the release of stored calcium (Berridge, 1993). Recently it has been shown that the co-agonist properties of Ca^{2+} and IP_3 in regulating the IP_3R (Bezprozvanny et al., 1991; Finch et al., 1991) can explain Ca^{2+} oscillations in certain cell types (Keizer and De Young, 1992). In this explanation, the initial increase in cytosolic Ca^{2+} through the IP_3R rapidly activates further Ca^{2+} release, by binding to an activation site on the IP_3R. This is followed on a slower time scale by inactivation when Ca^{2+} binds to a second site on the IP_3R. The oscillation cycle is completed as the increased cytosolic Ca^{2+} concentration, $[Ca^{2+}]_{cyt}$, is then lowered and the ER lumen is refilled by ATP-dependent calcium pumps. This is followed by another cycle of calcium release and uptake as long as $[IP_3]$ remains between a lower threshold value, set by the level of $[Ca^{2+}]_{cyt}$ required for activation, and an upper threshold value, set by the level of $[Ca^{2+}]_{cyt}$ required for inactivation. The oscillations can be observed by using either fluorescent dyes or electrophysiological probes, and confocal microscopy has revealed a complex spatial structure of Ca^{2+} waves underlying these oscillations (Lechleiter et al., 1991; Lechleiter and Clapham, 1992; Girard and Clapham, 1993). Although Ca^{2+} waves have been observed in cells that express either ryanodine receptors (skeletal muscle), or a combination of ryanodine receptors and IP_3Rs (cardiac muscle, smooth muscle, sea urchin eggs, etc.) we restrict our present study to a consideration of cells such as *Xenopus laevis* oocytes, in which the IP_3R is known to be the dominant Ca^{2+} release channel from internal stores (Parys et al., 1994). Thus, in cardiac myocytes and sea urchin oocytes, where there is a mixture of IP_3R and ryanodine receptors, the mechanism of wave propagation will be different.

Attempts have been made to correlate the properties of IP_3-induced Ca^{2+} waves with the diffusion of either IP_3 or Ca^{2+} in the cytoplasm (Berridge, 1993; Rooney and Thomas, 1993; Jaffe, 1993). Recent experiments (Allbritton et al., 1992) have established that the binding of Ca^{2+} to stationary and mobile buffers in the cytoplasm has a strong influence on the rate of Ca^{2+} diffusion, lowering its diffusion constant by an order of magnitude or more from that in an aqueous solution of comparable viscosity. IP_3, on the other hand, diffuses quite rapidly in the cytoplasm (Allbritton et al., 1992). In fact, recent simulations of Ca^{2+} waves

Received for publication 10 April 1995 and in final form 8 August 1995.
Address reprint requests to Dr. Joel Keizer, Institute of Theoretical Dynamics, 2201 Academic Surge, University of California, Davis, CA 95616-8618. Tel.: 916-752-0938; Fax: 916-752-7297; E-mail: jekeizer@ucdavis.edu.

0006-3495/95/11/2139/00 $2.00

(Jafri and Keizer, 1994) imply a diminished role for Ca^{2+} diffusion in certain intracellular Ca^{2+} wave trains but a major role for IP_3 in setting the timing of Ca^{2+} release from the IP_3R. Related conclusions have been reached for intercellular Ca^{2+} waves as well (Sneyd et al., 1995). Because cytosolic Ca^{2+} buffers are responsible for slowing Ca^{2+} diffusion, understanding the effect of buffers on Ca^{2+} waves is clearly important, no less so because the dyes used to visualize Ca^{2+} waves are themselves high-affinity Ca^{2+} buffers.

In some cells, endogenous buffers sequester in excess of 99% of the total calcium in the cytoplasm. The buffer site concentrations in the cytosol, estimated to be in the range of 100–300 μM (Neher and Augustine, 1992; Tse et al., 1994) and higher in the ER (Milner et al., 1992), comprise both stationary and mobile calcium-binding proteins. Others (Zhou and Neher, 1993) have estimated that as much as 25% of cytoplasmic buffers in chromaffin cells are mobile, whereas the remainder are relatively stationary. The local distribution of bound calcium between the two types of buffers is determined by the association dissociation equilibrium of Ca^{2+} with the buffers, which have time constants estimated to be in the millisecond range or smaller (Neher and Augustine, 1992; Zhou and Neher, 1993). Stationary buffers tend to retard the diffusion of Ca^{2+}, whereas mobile buffers (including fluorescent indicators like fura-2) increase the transport of Ca^{2+}. When the association-dissociation equilibrium is sufficiently rapid, a single transport equation that takes into account the effect of buffers on diffusion and the rapid sequestering of free Ca^{2+} can be used to describe Ca^{2+} transport (Wagner and Keizer, 1994). Buffering can also indirectly alter the kinetics of Ca^{2+} handling by the ER (Wagner and Keizer, 1994; Jafri et al., 1992).

Experiments have shown that the ER plays an active role in Ca^{2+} waves. For example, in mouse eggs the Ca^{2+} wave induced by sperm-egg fusion is eliminated by the injection of monoclonal antibodies to the IP_3R (Miyazaki et al., 1992), which is the major Ca^{2+} release channel in those cells. Similarly, in immature *Xenopus laevis* oocytes, which utilize the SERCA2 Ca^{2+}-ATPase, artificial expression of the SERCA1 isoform increases the frequency of the IP_3-induced waves, whereas the wavelength remains roughly constant (Camacho and Lechleiter, 1993). Thapsigargin and ionomycin, which inhibit SERCA pumps and increase the leak of Ca^{2+} from the ER, respectively, are also known to effect IP_3-induced Ca^{2+} oscillations (Li et al., 1994). Finally, cortical ER preparations from sea urchin eggs exhibit a traveling wave of Ca^{2+} depletion when stimulated by IP_3 (Terasaki and Sardet, 1991). Thus diffusion, the buffering of Ca^{2+}, and the ER all play significant roles in cytosolic Ca^{2+} waves.

Previous theoretical studies of calcium waves have used either discrete cellular automaton models (Lechleiter et al., 1991) or reaction diffusion mechanisms (Girard et al., 1992; Dupont and Goldbeter, 1992; Atri et al., 1993; Jafri, 1995) that ignore the effects of both mobile and stationary buffers and the distribution of Ca^{2+} in the ER lumen. Those studies have concentrated on the mechanism of propagation of spiral waves or solitary trigger waves initiated by a pulse of IP_3 or Ca^{2+} at resting $[IP_3]$ below the threshold for oscillations. Here we expand on our previous study of Ca^{2+} waves (Jafri and Keizer, 1994) that includes both stationary and mobile buffers as well as changes in lumenal Ca^{2+}, to explore a variety of effects involving diffusion, buffers, and ER Ca^{2+} handling. We rely on the rapid equilibration theory (Wagner and Keizer, 1994) to describe buffering. This is then combined with mechanisms in the ER and cytoplasm that include a simplification of the model of the IP_3-receptor Ca^{2+} channel (De Young and Keizer, 1992; Keizer and De Young, 1994), diffusion of calcium in the cytosol and ER, and the breakdown and diffusion of IP_3.

MECHANISMS

Our mechanism for simulating Ca^{2+} waves is based on the ideas of De Young and Keizer (De Young and Keizer, 1992; Keizer and De Young, 1994) for IP_3-linked Ca^{2+} oscillations (see Fig. 1). Like the original model, Ca^{2+} release from the ER is initiated by the rapid activation of the IP_3R by IP_3 and Ca^{2+} and terminated by slow inhibition by Ca^{2+}. The ER is refilled by a SERCA Ca^{2+} pump, Ca^{2+} leaks passively out of the ER, and IP_3 is degraded to a steady-state level. Ca^{2+} bound buffers are denoted in Fig. 1 by $[CaB_j]$, where $j = s, m, e$ represents stationary, mobile, and exogenous buffers, respectively. Our present calculations use a reduced version of the model for the IP_3R that involves the

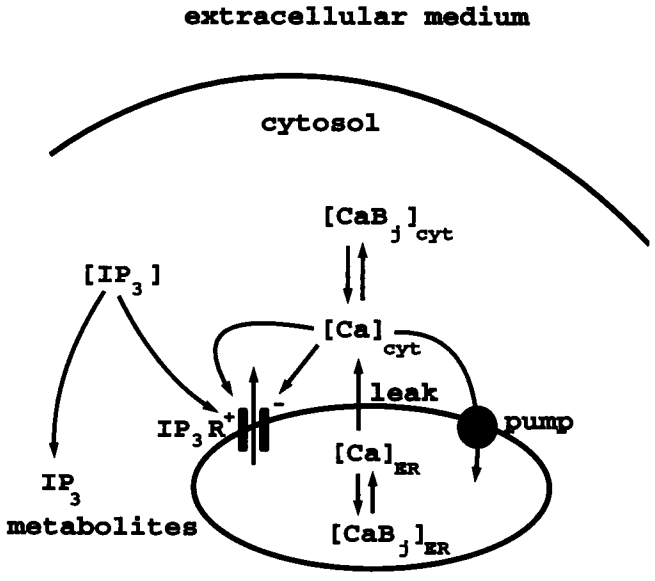

FIGURE 1 Schematic diagram of mechanisms included in calculations of Ca^{2+} waves. Ca^{2+} release from the ER into the cytosol occurs via the IP_3R, which is regulated by the co-agonist properties of IP_3 and Ca^{2+} (+ for activation, − for inhibition) and a passive leak. Uptake into the ER is via SERCA Ca^{2+}-ATPase pumps. IP_3 is produced and degraded via phospholipid metabolism, and Ca^{2+} is bound to mobile and stationary buffers, B_j.

dynamic modeling of only two states of the receptor (Keizer and De Young, 1994). Fig. 2 shows the three states of the IP_3R, i.e., closed, open, and inactivated. Only transitions to and from the open and closed states appear in the kinetic equations. The variable $X_{i,j,k}$ represents the fraction of the four subunits of the IP_3R (assumed identical) that have i = 0 or 1 IP_3 molecule bound; j = 0 or 1 activating Ca^{2+} bound; and k = 0 or 1 inactivating Ca^{2+} bound. The binding of IP_3 is known to be rapid and is assumed to be at equilibrium. The present model (Jafri and Keizer, 1994) also includes the following additional features: 1) diffusion of IP_3 in the cytosolic compartment, 2) diffusion of Ca^{2+} in the ER lumen, 3) diffusion of Ca^{2+} in the cytosolic compartment, 4) buffering of Ca^{2+} in the cytosolic compartment, and 5) buffering of Ca^{2+} in the ER lumen.

The model makes the following assumptions: 1) The ER is a homogeneous, continuous medium. 2) The buffers are assumed to possess only one binding site for Ca^{2+}. 3) Extracellular Ca^{2+} is not necessary for Ca^{2+} wave propagation, although it can be easily added and can modify the frequency and velocity of waves (Jafri, 1995; Atri et al., 1993; Girard and Clapham, 1993).

DIFFERENTIAL EQUATIONS

The model consists of five differential equations for five dynamical variables: 1) the cytosolic calcium concentration ($[Ca^{2+}]_{cyt}$), 2) the ER calcium concentration ($[Ca^{2+}]_{ER}$), 3) the cytosolic IP_3 concentration ($[IP_3]$), 4) the fraction of IP_3R subunits in the closed state with only IP_3 bound (X_{100}), and 5) the fraction of subunits in the open state with both IP_3 and an activating Ca^{2+} bound (X_{110}). Parameter definitions and their values are given in Tables 1–3.

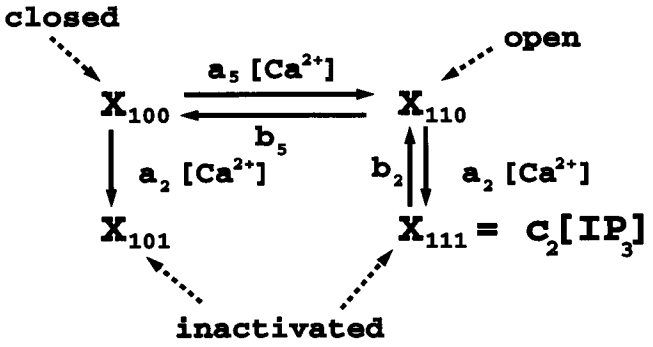

FIGURE 2 The reduced model governing the fraction (X) of IP_3R subunits in various states. The states are designated 100 (closed), 110 (open), and 101 and 111 (inactivated). Binding of Ca^{2+} to its activation site opens the channel, and binding to its inactivation site closes the channel. In the reduced model $X_{111} = c_2[IP_3]$. A subunit of the IP_3-receptor channel is approximated by two states, X_{100} (closed) and X_{110} (open). The channel converts from the closed to open state by the binding of calcium to the activation site. The channel can inactivate by calcium binding to another site. The resting fraction of the inactivated channel with IP_3 bound is assumed to be proportional to $[IP_3]$.

TABLE 1 Ca^{2+} regulatory mechanism parameters

Parameter	Definition	Value
c_1	Ratio of ER volume to cytosolic volume	0.185
c_2	Proportionality constant of X_{111} to $[IP_3]$	0.2 μM
v_1	Maximum IP_3 receptor flux	300 s^{-1}
v_2	Ca^{2+} leak rate constant	2.0 s^{-1}
v_3	SERCA2 maximal pump rate	45.0 $\mu M\,s^{-1}$
v_6	SERCA1 maximal pump rate	0.0 $\mu M\,s^{-1}$
k_3	SERCA2 dissociation constant	0.1 μM
k_6	SERCA1 dissociation constant	0.4 μM
a_2	Inhibitory receptor binding constant	0.2 $\mu M^{-1}\,s^{-1}$
a_5	Activation receptor binding constant	20.0 $\mu M^{-1}\,s^{-1}$
d_2	Inhibitory receptor dissociation constant	1.0 μM
d_5	Activation receptor dissociation constant	82.3 nM
$[IP_3]$*	Basal concentration of IP_3	0.26 μM

The balance equation for $[Ca^{2+}]_{cyt}$ based on Fig. 1 is

$$\frac{\partial[Ca^{2+}]_{cyt}}{\partial t} = \beta_{cyt}\Big[(D_{Ca}^{cyt} + \gamma_m^{cyt}D_m^{cyt} + \gamma_e^{cyt}D_e^{cyt})\nabla^2[Ca^{2+}]_{cyt} - 2\left\{\frac{\gamma_m^{cyt}D_m^{cyt}}{K_m^{cyt} + [Ca]_{cyt}} + \frac{\gamma_e^{cyt}D_e^{cyt}}{K_e^{cyt} + [Ca]_{cyt}}\right\}\nabla[Ca]_{cyt}\cdot\nabla[Ca]_{cyt} \quad (1)$$

$$+ c_1(v_2 + v_1X_{110}^3)([Ca^{2+}]_{ER} - [Ca^{2+}]_{cyt}) - \frac{v_3[Ca^{2+}]_{cyt}^2}{[Ca^{2+}]_{cyt}^2 + k_3^2}\Big],$$

where

$$\beta_{cyt} = \left\{1 + \frac{[B_s]_{cyt}K_s^{cyt}}{(K_s^{cyt} + [Ca^{2+}]_{cyt})^2} + \frac{[B_m]_{cyt}K_m^{cyt}}{(K_m^{cyt} + [Ca^{2+}]_{cyt})^2} + \frac{[B_e]_{cyt}K_e^{cyt}}{(K_e^{cyt} + [Ca^{2+}]_{cyt})^2}\right\}^{-1} \quad (2)$$

and

$$\gamma_l^{cyt} = \frac{[B_l]_{cyt}K_l^{cyt}}{(K_l^{cyt} + [Ca]_{cyt})^2}, \quad (3)$$

TABLE 2 Ca^{2+} buffering parameters

Parameter	Definition	Value
$[B_s]_{cyt}$	Total cytosolic stationary buffer concentration	225.0 μM
$[B_m]_{cyt}$	Total cytosolic mobile buffer concentration	75.0 μM
K_s^{ER}	Stationary buffer dissociation constant in the ER	10.0 μM
K_m^{ER}	Mobile buffer dissociation constant for Ca^{2+} in the ER	6.0 μM
$[B_s]_{ER}$	Total stationary buffer concentration in the ER	100 mM
$[B_m]_{ER}$	Total mobile buffer concentration in the ER	250 μM
$[B_e]_{cyt}$	Total exogenous mobile buffer concentration in the cytosol	0.0 μM
K_s^{cyt}	Cytosolic stationary buffer dissociation constant for Ca^{2+}	1 mM
K_m^{cyt}	Cytosolic mobile buffer dissociation constant for Ca^{2+}	6.0 μM
K_e^{cyt}	Exogenous mobile buffer dissociation constant for Ca^{2+} in the cytosol	0.16 μM

TABLE 3 Diffusion constants

Parameter	Definition	Value ($\mu m^2 \cdot s^{-1}$)
D_{Ca}^{ER}	Calcium diffusion constant in the ER	223
D_{Ca}^{cyt}	Calcium diffusion constant in the cytosol	223
D_m^{ER}	Mobile buffer diffusion constant in the ER	75.0
D_m^{cyt}	Mobile buffer diffusion constant in the cytosol	75.0
D_e^{cyt}	Exogenous mobile buffer diffusion constant in the cytosol	75.0
D_{IP_3}	Diffusion constant for IP_3	283

These values are used in all simulations unless stated in the figure legends. The initial conditions used are $[Ca]_{cyt} = 0.0845\ \mu M$, $[Ca]_{ER} = 10.891\ \mu M$, $[IP_3] = 0.23\ \mu M$, $X_{100} = 0.281$, $X_{110} = 0.291$ for trigger waves, and $[Ca]_{cyt} = 0.0537\ \mu M$, $[Ca]_{ER} = 10.947\ \mu M$, $[IP_3] = 0.28\ \mu M$, $X_{100} = 0.329$, $X_{110} = 0.216$ for suprathreshold waves unless otherwise specified.

with $l = m$ or e and the total concentrations of the stationary (s) and mobile (m) endogenous and exogenous (e) buffers are represented by $[B_i]_{cyt}$ (i = s, m, e). The term β_{cyt} is the differential fraction of free Ca^{2+} in the cytoplasm.

The first term inside the square brackets of Eq. 1 describes a diffusive-type transport of Ca^{2+} in the cytosol; the second term is due to the uptake of Ca^{2+} by mobile buffers as free Ca^{2+} moves down its gradient and is a nondiffusive term; the third term combines the leak flux (v_2) and the IP_3R flux (v_1) across the ER membrane; and the fourth term represents the SERCA pump. For the standard parameters in Table 3 the nondiffusive transport of Ca^{2+} is small compared to the other fluxes. Although the rapid buffer approximation that is used to describe buffering is not valid for very small distance scales, for buffers with equilibration times of the order of milliseconds the approximation is quite good for distance scales larger than a few microns (Wagner and Keizer, 1994). Because this is below the limit of resolution of large-scale confocal imaging of Ca^{2+} waves, use of the rapid buffering approximation seems justified.

The balance equation for $[Ca^{2+}]_{ER}$ is

$$\frac{\partial [Ca^{2+}]_{ER}}{\partial t} = (1/c_1)\beta_{ER}\Bigg[\Bigg\{(D_{Ca}^{ER} + \gamma_m^{ER} D_m^{ER})\nabla^2[Ca^{2+}]_{ER} - 2\frac{\gamma_m^{ER} D_m^{ER}}{K_m^{ER} + [Ca]_{ER}}\nabla[Ca]_{ER} \cdot \nabla[Ca]_{ER}\Bigg\}c_1 - c_1(v_2 + v_1 X_{110}^3) \times ([Ca^{2+}]_{ER} - [Ca^{2+}]_{cyt}) + \frac{v_3[Ca^{2+}]_{cyt}^2}{[Ca^{2+}]_{cyt}^2 + k_3^2}\Bigg], \quad (4)$$

where

$$\beta_{ER} = \left\{1 + \frac{[B_s]_{ER} K_s^{ER}}{(K_s^{ER} + [Ca^{2+}]_{ER})^2} + \frac{[B_m]_{ER} K_m^{ER}}{(K_m^{ER} + [Ca^{2+}]_{ER})^2}\right\}^{-1} \quad (5)$$

and

$$\gamma_m^{ER} = \frac{[B_m]_{ER} K_m^{ER}}{(K_m^{ER} + [Ca]_{ER})^2}. \quad (6)$$

For calculations in which the expression of SERCA1 Ca^{2+}-ATPase is simulated, the term

$$\beta_{cyt}\left\{\frac{v_6[Ca^{2+}]_{cyt}^2}{[Ca^{2+}]_{cyt}^2 + k_6^2}\right\} \quad (7)$$

is subtracted and added inside the square brackets of Eqs. 1 and 4, respectively.

The production, degradation, and diffusion of IP_3 are described by

$$\frac{\partial [IP_3]}{\partial t} = D_{IP_3}\nabla^2[IP_3] + I_f([IP_3]^* - [IP_3]). \quad (8)$$

The steady-state level of IP_3, denoted $[IP_3]^*$, is assumed to remain elevated above zero because of the basal level of IP_3 production. Finally, the states of the IP_3 receptor Ca^{2+} channel satisfy the following equations:

$$\frac{dX_{100}}{dt} = -a_2[Ca^{2+}]_{cyt}X_{100} - a_5[Ca^{2+}]_{cyt}X_{100} + b_5X_{110} \quad (9)$$

$$\frac{dX_{110}}{dt} = -a_2[Ca^{2+}]_{cyt}X_{110} + b_2c_2[IP_3] + a_5[Ca^{2+}]_{cyt}X_{100} - b_5X_{110}, \quad (10)$$

where X_{100} and X_{110} are the fraction of channels in the closed and open states, respectively (Keizer and De Young, 1994). The arrows in Fig. 2 show the steps that convert the various states.

The system of five coupled differential equations was solved on a Silicon Graphics Indigo workstation using an implicit finite difference method on a linear grid in one dimension (Ames, 1977). Two-dimensional calculations were carried out on a Silicon Graphics Onyx or Indigo workstation and used an implicit finite difference method with local operator splitting (Ames, 1977; Lapidus and Pinder, 1982). In this method, the solution is computed by solving a fractional time step in one space dimension and then another fractional time step in the other so that the sum of the time steps approximates a complete time step. No flux boundary conditions were used for all mobile species. Graphics were generated using PV-WAVE by Precision Visuals, Inc.

SELECTION OF PARAMETERS

The standard parameter values used in the simulations are given in Tables 1–3, unless specified in the figure legends or text. Table 1 gives the parameters of the DeYoung and Keizer model (De Young and Keizer, 1992), in which v_1 and v_3 have been rescaled by a factor of 50 to account for the fact that Ca^{2+} buffers are explicitly included in our simulations. The dissociation constant for SERCA1 was taken from experiment (Lytton et al., 1992). The Ca^{2+} buffering parameters in Table 2 are typical of those measured in *Xenopus laevis* cytoplasm and the ER (Allbritton et al., 1992; Somlyo et al., 1985; Wagner and Keizer, 1994).

The parameters for diffusion are given in Table 3 and were obtained from previous work (Allbritton et al., 1992; Wagner and Keizer, 1994). In the following discussion of results, "no calcium diffusion" means that $D_{Ca}^{ER} = D_{Ca}^{cyt} = D_{m}^{cyt} = D_{m}^{ER} = D_{e}^{cyt} = 0$ ($J_{dif} = J_{dif}^{ER} = 0$).

Calcium waves are seen in response to the introduction of Ca^{2+}, IP_3, or its nonhydrolyzable analogues into the cytoplasm (Lechleiter et al., 1991; Nuccitelli et al., 1993). In living cells, this can be performed by injection or release of a caged compound introduced into the cell. Additionally, IP_3 can be produced by agonist stimulation and Ca^{2+} can be increased through plasmalemmal Ca^{2+} channels. In our simulations Ca^{2+} injections are mimicked by using an initial square 4.0 μM pulse of Ca^{2+} in the left 30 μm of the domain. Injection of IP_3 is simulated by an initial 10 μM square pulse of IP_3 at the left 5 μm of the domain. Solitary trigger waves are generated at steady-state $[IP_3]$ below the threshold for oscillations ($[IP_3]^* = 0.245$ μM). For trigger waves the time step $dt = 0.01$ s and the space step $dx = 0.1$ μm. Wave trains (in one dimension) and target patterns and spiral waves (in two dimensions) are generated when ($[IP_3]^* > 0.25$ μM). For those simulations $dt = 0.02$ s and $dx = 0.1$ μm ($dx = 1.0$ μm for two-dimensional simulations). One-dimensional simulations were performed on a 500-μm line and the two-dimensional simulations were performed on a 250 μm by 250 μm square.

Wave trains were also generated by an initial linear ramp of $[IP_3]$ that declined from the left-hand side of the spatial domain. In those simulations after a time interval several times larger than the IP_3 degradation time, $1/I_r$, the ramp of $[IP_3]$ relaxes to a uniform value, $[IP_3]^*$. There is some variability in time and space for the wave speed, width, and amplitude of wave trains initiated using ramps or pulses of IP_3. This is due to the fact that these waves have a high degree of kinematic character (Jafri and Keizer, 1994). This is illustrated in Fig. 3, which shows results of measurements of these quantities at different points and times compared to $1/I_r$ for an initial ramp of $[IP_3]$ equal to 2.75 μM at the left boundary and 0.25 μM at the right boundary. Note that the wave amplitude decreases slightly from left to right whereas the wave speed and width decrease away from the left boundary and level off near 200 μm. Therefore, in the simulations the wave speed, wavelength, wave width, and amplitude were measured at a point more than 200 μm from the left boundary.

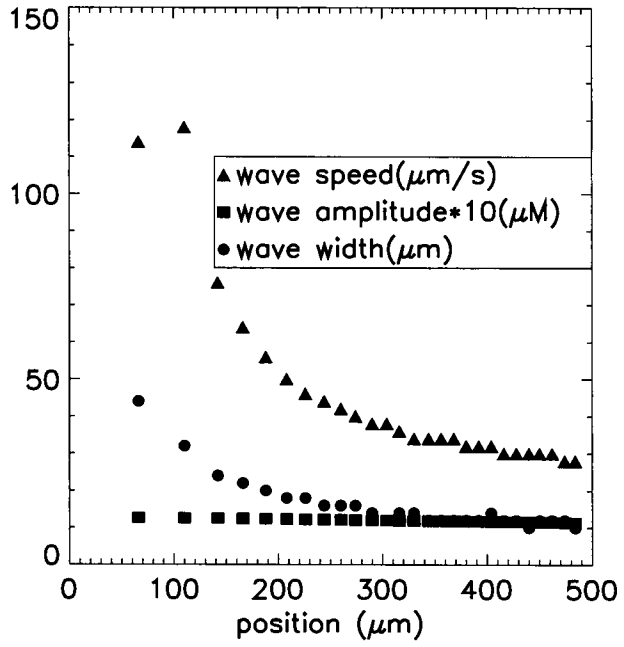

FIGURE 3 Wave trains generated by an initial linear ramp of IP_3 (2.75 μM at position $x = 0$ μm and 0.25 μM at $x = 500$ μm) have characteristics that depend on position. For $x \geq 200$ μm, the wave properties are relatively constant.

ROLE OF DIFFUSION

We have carried out simulations in one and two dimensions with the resulting Ca^{2+} waves falling into three broad categories: solitary trigger waves, wave trains, and spiral waves (Murray, 1990). Trigger waves require diffusion for their propagation and can be initiated by a pulse of Ca^{2+} or IP_3 if the cytoplasm is below the threshold for Ca^{2+} oscillations and "excitable." The term "excitable" refers to the fact that the equations (or the cytoplasm that they represent) can exhibit a transient, action-potential-like spike of cytosolic Ca^{2+}. Such a transient spike can be initiated by a sufficiently large perturbation of the stable steady state by either Ca^{2+} or IP_3. The resulting spike momentarily excites Ca^{2+} release from a localized region of the ER and gives rise to a solitary, propagating trigger wave. Larger perturbations sometimes produce a transient train of waves. In two dimensions an excitable cytoplasm can also support stable spiral waves. Repetitive wave trains, on the other hand, occur when the cytoplasm is oscillatory, that is, when conditions are adjusted so that in the absence of diffusion Ca^{2+} oscillations would occur spontaneously. These repetitive wave trains are generated in both our one- and two-dimensional calculations, the latter taking the appearance of target patterns and spiral waves. In our calculations the nature of the wave trains has only a weak dependence on the diffusion of Ca^{2+}. Because an actual physical movement of Ca^{2+} is not required for these wave trains, they are termed "kinematic" or "phase" waves (Kopell and Howard, 1973; Ross et al., 1988; Murray, 1990; Jafri and Keizer, 1994). The idea underlying phase waves is explained in more detail below (cf. Fig. 6).

Trigger waves

Here we summarize the results of one-dimensional simulations when $[IP_3]^*$ is set in the excitable regime, just below the threshold for oscillations ($[IP_3]^* = 0.245$ μM). In this regime a solitary trigger wave of Ca^{2+} can be produced when the cytoplasm is given a square wave pulse of Ca^{2+}

($\approx$1.0 μM) in the left 30 μm of the domain. Such a wave moves toward the right and propagates across the entire domain. Similarly, a short train of trigger waves can be generated by stimulation with a 10 μM pulse of IP_3 in the left 5 μm of the domain. A typical wave is shown in Fig. 4 at t = 32 s. As found with other trigger waves in excitable media (Murray, 1990), the wave form and wave speed remain invariant as the wave propagates from left to right. The existence of stable trigger waves in excitable media is well known (Murray, 1990) to be dependent upon diffusion of one or more excitatory substances, and we have verified that when there is no calcium diffusion, trigger waves cannot be generated. This is despite the fact that the Ca^{2+} flux due to diffusion (first and second terms in Eq. 1; shown as J_{dif} in Fig. 4) is considerably smaller than the fluxes due to ER Ca^{2+} handling (third and fourth terms in Eq. 1; shown as $J_{channel+leak}$ and J_{pump}). Indeed, when J_{dif} and J_{dif}^{ER} are set equal to zero and the simulation in Fig. 4 is continued further, the Ca^{2+} wave rapidly dissipates. The effect of buffering on trigger waves and the influence of buffering on diffusion are treated in subsequent sections.

Repetitive wave trains

During periods of agonist stimulation when $[IP_3]$ is elevated, Ca^{2+} oscillations and Ca^{2+} wave trains can be observed in vivo (Lechleiter et al., 1991). Oscillations continue as long as $[IP_3]$ remains above the oscillatory threshold. Previously, we simulated this situation by applying a 10 μM pulse of IP_3 at the left 5 μm of the domain when $[IP_3]^*$ is set just above the threshold for oscillations (Jafri and Keizer, 1994). In Fig. 5 *A*, a 4.0 μM pulse of Ca^{2+} in the left 30 μm yields an initial wave that terminates as it encounters a bulk oscillation of the cytosol to the right of the wave. The next wave in the train, however, propagates further to the right before it also terminates in a bulk oscillation. The distance the initial wave travels depends upon the size of the initial Ca^{2+} pulse, and the frequency of the oscillations is determined by $[IP_3]^*$. All subsequent waves propagate farther until the waves propagate all the way to the right boundary, which they continue doing for the remainder of the simulation (410 s). Although the diffusion flux in this case is approximately the same size as that for the trigger wave in Fig. 4, it turns out not to be essential for the propagation of the wave train.

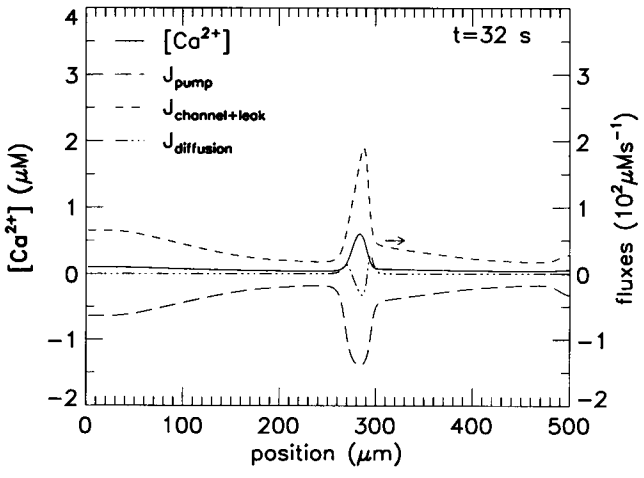

FIGURE 4 A Ca^{2+} trigger wave propagates to the right in response to a 10 μM pulse of IP_3 in the left 5 μm of the domain. The fluxes are scaled to show their contribution after buffering. $[IP_3]^*$ = 0.245 μM, below the threshold for oscillations. The wave velocity is 12 $\mu m \cdot s^{-1}$.

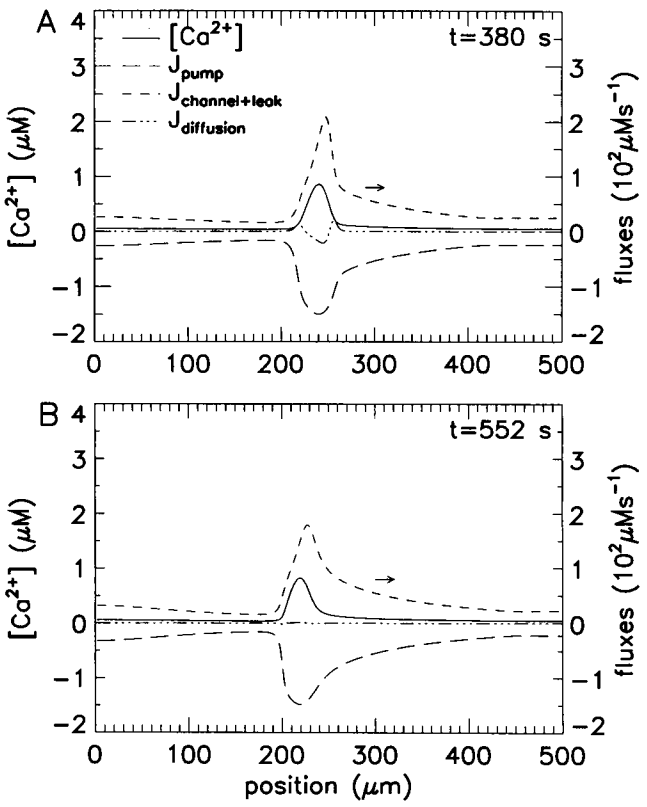

FIGURE 5 A Ca^{2+} wave train propagates to the right in response to a 4.0 μM pulse of Ca^{2+} in the left 30 μm of the domain with $[IP_3]^*$ = 0.26 μM. (*A*) Diffusion of Ca^{2+} is required for the first wave to propagate across the domain (t = 380 s). (*B*) Subsequent waves propagate in the absence of Ca^{2+} diffusion after t = 410 s (t = 552 s shown). In both (*A*) and (*B*) the wave velocity is 10 $\mu m \cdot s^{-1}$.

To see the role that diffusion actually plays in wave train propagation, all diffusion processes in Eqs. 1 and 4 involving $[Ca^{2+}]_{cyt}$ and $[Ca^{2+}]_{ER}$ were set to zero, and the simulation in Fig. 5 *A* was continued (Fig. 5 *B*). In contrast to what was observed for trigger waves, a wave train continues to propagates across the domain from the left. The wave profile is slightly different from the previous case, in that the ER Ca^{2+} fluxes are somewhat larger at the front of the wave, and that $J_{dif} = J_{dif}^{ER} = 0$. Qualitatively similar behavior is seen for other levels of stimulation and parameters above the threshold for oscillations. The differences between the Ca^{2+}- and IP_3-induced waves are due to differences in the levels of stimulation.

Clearly these waves do not require diffusion to propagate, although diffusion does contribute to their shape. In this

sense they are distinct from trigger waves. Waves that propagate in the absence of diffusion are called "kinematic" or "phase" waves (Kopell and Howard, 1973; Murray, 1990). True kinematic waves are caused by either small differences in the phases of spatially adjacent oscillators or small differences in their frequencies. No matter is actually transported in kinematic waves. The Ca^{2+} wave trains in Fig. 5 are caused predominately by differences in phase due to the passage of the original trigger wave across the spatial domain. Little Ca^{2+} is actually transported during the passage of a wave because the diffusion of Ca^{2+} is slow.

The nature of a phase wave is illustrated in Fig. 6, where a simulation has been carried out with no Ca^{2+} diffusion, but with a spatial distribution of phases. Focusing on positions 100, 120, 140, 160, and 180 μm, notice that each oscillator is slightly ahead in phase of the oscillator directly to its right. This means that an oscillator will reach its peak amplitude immediately before the oscillator to the right. As time progresses the location of the peak amplitude moves to the right and it appears that a wave has passed. The top panel of Fig. 6 shows the spatial profile of the wave at time t = 150 s (see dashed line in bottom panels). The points *A*, *B*, *C*, *D*, and *E* on the spatial profile correspond to points on the time series. Examination of the figure shows that at $t \approx$ 158 s the peak of the kinematic wave will have propagated to point *E*.

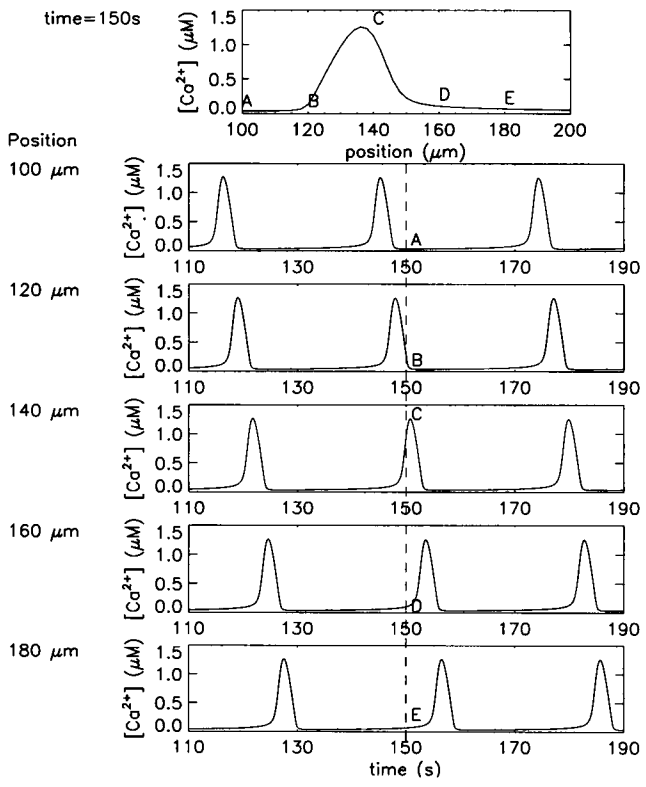

FIGURE 6 (*Top*) A phase wave without Ca^{2+} diffusion. The wave consists of independent oscillators at each point that are slightly staggered in phase. (*Bottom*) The time course of $[Ca^{2+}]_{cyt}$ at the positions denoted by A–E (100, 120, 140, 160, and 180 μm). The vertical dotted line at t = 150 s corresponds to the wave in the top panel. The wave was generated by a ramp as in Fig. 3 with $[IP_3]^*$ = 0.36 μM.

The differences in phase (phase gradient) that are required for these oscillations can be set by an initial pulse or ramp of IP_3. In fact, any spatial inhomogeneity of $[IP_3]$ will suffice to establish a phase gradient. In cells IP_3 injection or release of caged IP_3 is commonly used for the generation of waves (Lechleiter and Clapham, 1992). Because IP_3 diffuses so much faster than Ca^{2+}, it can rapidly transmit a signal across a cell. This IP_3 signal is then transduced into the phase differences that contain the information for the wavelength and speed of the wave. The first wave that passes in response to a pulse of calcium also can set the phase gradient, but at a slower rate than IP_3. The elevated IP_3 signal decays after a short period (ca. 50 s in our simulations). The information from the signal, however, remains stored in the phase gradient, and the wave train continues to propagate away from the peak of the original $[IP_3]$. Alternatively, any propagating wave (even a trigger wave) will set the phase of the media in its wake, which may account for the constantly changing pattern of waves seen in *Xenopus laevis* oocytes.

Previously (Jafri and Keizer, 1994) we have used initial ramps of IP_3 to initiate wave trains, and found that the wavelength (λ) and speed (c) vary systematically with the period (τ) of the oscillations, which is set by the value of $[IP_3]^*$. In the oscillatory regime we found the linear dispersion relationship, $c = \lambda/\tau$, which would be expected to hold for kinematic waves, to be approximately valid for our simulations. This is illustrated for the standard parameters, with and without Ca^{2+} diffusion, by the points for $v_6 = 0$ and the line with slope $1/\tau$ in Fig. 7.

Circular and spiral waves

Confocal microscopy enables Ca^{2+} waves to be observed in a nearly flat, confocal plane. Observations of this sort in immature *Xenopus laevis* have yielded a rich structure of dynamic patterns, including circular target waves and spiral waves (Lechleiter et al., 1991; Lechleiter and Clapham, 1992). In an attempt to mimic these phenomena (Girard et al., 1992; Atri et al., 1993), we have carried out two-dimensional simulations in a square domain using various type of pulses and initial conditions to stimulate Ca^{2+} waves. Circular Ca^{2+} waves were easily generated from square pulses of Ca^{2+} at the center of the domain. These are the analogue of plane waves generated in one dimension. As found in our one-dimensional simulations, waves generated just below the threshold for Ca^{2+} oscillations consisted of either a solitary circular wave or a transient wave train, depending on the size of the initial stimulus. Moving target patterns, the analogue of one-dimensional wave trains, are generated above the oscillation threshold. Just as we found in our one-dimensional simulations, diffusion of Ca^{2+} is essential for the propagation of subthreshold circular waves, although terminating all diffusion ($J_{dif} = J_{dif}^{ER} = 0$) of Ca^{2+} does not affect repetitive wave propagation.

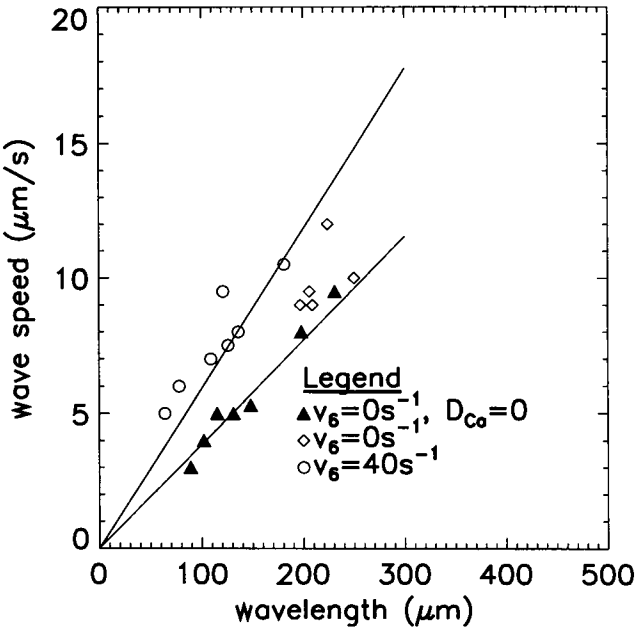

FIGURE 7 The wavelength (λ) vs wave speed (c) for a series of linear ramps with differing slopes are related by the equation $c = \lambda/\tau$, where τ is the period of the oscillations. Data generated by various ramps of initial $[IP_3]$ show that the period of the oscillations decreases with increasing SERCA1 expression, which is represented by an increase in the SERCA1 maximal pump rate (v_6). The lines shown have slope $1/\tau$ where the average periods (τ) are 26 s and 16.9 s, for $v_6 = 0$ $\mu M \cdot s^{-1}$ and 40 $\mu M \cdot s^{-1}$, respectively ($[IP_3]^* = 0.36$ μM). The data were obtained from sets of two waves with constant wavelengths and wave speeds from both waves in all three sets. The wavelength is the distance between the two waves in each set.

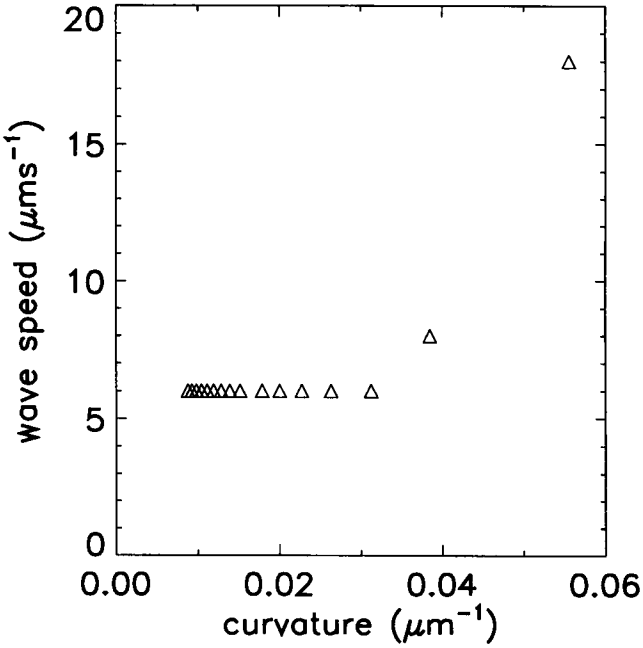

FIGURE 8 Dependence of the wave speed on the curvature ($\kappa = 1/r$) for a circular trigger wave ($[IP_3]^* = 0.245$ μM). At high curvature (low radius), the wave speed is elevated because of the elevated level of Ca^{2+} from the initiating pulse. Distances are measured to ± 1 μm.

We have measured the speed of these waves as a function of the distance of their wave front from their center, r, and plotted this as a function of the curvature of the wave front, $\kappa = 1/r$. For subthreshold waves ($[IP_3]^* = 0.245$ μM), Fig. 8 shows that the wave speed is nearly independent of the curvature below $\kappa = 0.03$ μm^{-1} and rises sharply near the radius of the initiating pulse. Comparable results are found for suprathreshold target waves. This differs from other theoretical predictions for the curvature dependence of the wave speed for other excitable reaction diffusion systems (Keener and Tyson, 1986; Sneyd and Atri, 1993). We have also investigated the critical radius for generation of solitary circular traveling waves (Keener and Tyson, 1986) by using square pulses of Ca^{2+} with smaller amplitudes and width. Below widths of approximately 9–10 μm it is not possible to activate a wave using a pulse amplitude equal to that of the propagating wave. Additional simulations show that this does not depend strongly upon $[IP_3]^*$. This suggests a critical radius of 9–10 μm, which is comparable to that estimated in *Xenopus laevis* oocytes (Lechleiter and Clapham, 1992), despite the fact that the curvature dependence of the simulated waves in Fig. 8 differs somewhat from that measured experimentally.

By perturbing the medium into which a circular wave propagates, it is possible to generate spiral waves when the medium is below the oscillation threshold. Such waves continue to propagate as spirals even after IP_3 is elevated into the oscillatory regime, as shown in Fig. 9, which shows a subthreshold spiral after elevating $[IP_3]^*$ from 0.245 to 0.36 μM. Calcium diffusion is essential for continued propagation of spiral waves, in both the excitable and oscillatory regimes. In the excitable regime, terminating diffusion causes the wave to dissipate rapidly. In the oscillatory regime, on the other hand, setting Ca^{2+} diffusion equal to zero causes the organizing center of the spiral, which is smaller than the critical radius, to destabilize and change into a center for a target pattern. This is shown in Fig. 10, which is a continuation of the calculation in Fig. 9, but with no Ca^{2+} diffusion.

ROLE OF THE ER

The fluxes of Ca^{2+} in Figs. 4 and 5 show that both trigger waves and wave trains involve localized cycles of Ca^{2+} uptake and release by the ER. These fluxes, in fact, are essential to the maintenance of excitability and oscillations. Indeed, if either the influx rate through the SERCA pump or the efflux rate through the IP_3R is reduced sufficiently (say, by thapsigargin or monoclonal antibodies, respectively) IP_3-induced oscillations and waves can be terminated (Miyazaki et al., 1992). This is also true in our simulations, for which a sufficient decrease in either of these fluxes by lowering the parameters v_3 or v_1 terminates both trigger waves and wave trains.

Because of the importance of Ca^{2+} handling by the ER, it is not surprising that Ca^{2+} waves in the cytosol are

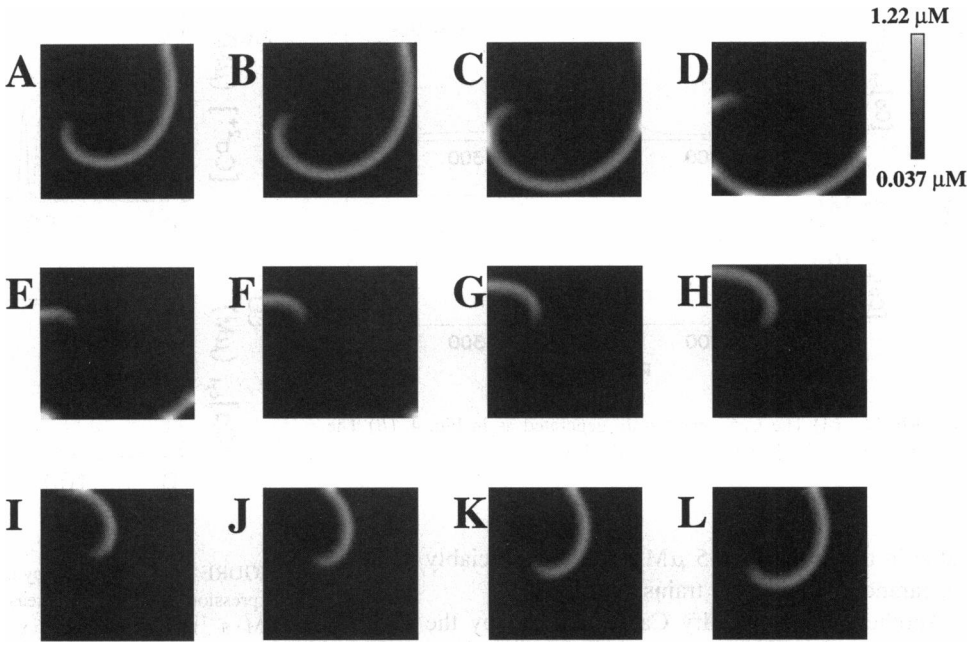

FIGURE 9 A stable spiral wave in the oscillatory regime ($[IP_3]$ = 0.36 μM) (250 μm by 250 μm). The spiral was initiated below threshold ($[IP_3]^*$ = 0.245 μM) by two 4 μM Ca^{2+} pulses (at the upper right corner and the middle of the left side) with refractory blocks to break the wave front. $[IP_3]^*$ was then elevated at t = 200 s. Frame *A* starts at t = 266 s with 3-s intervals between frames. The initial conditions were $[Ca]_{cyt}$ = 0.0845 μM, $[Ca]_{ER}$ = 10.891 μM, $[IP_3]$ = 0.23 μM, X_{100} = 0.281, X_{110} = 0.291, except in the refractory region, where $[Ca]_{cyt}$ = 0.50 μM, $[Ca]_{ER}$ = 10.07 μM, $[IP_3]$ = 0.245 μM, X_{100} = 0.06, X_{110} = 0.37.

accompanied by depletion waves in the ER, as shown for a plane wave in Fig. 11. These waves are similar to the waves of decreased fluorescence observed in sea urchin cortices that have been loaded with fluo-3/AM and stimulated by IP_3 (Terasaki and Sardet, 1991). Above the threshold for Ca^{2+} oscillations, where Ca^{2+} diffusion in the cytosol is much less important, coupling between the cytosolic wave and the depletion wave is quite tight, as is apparent from the differential Eqs. 1 and 4.

The coupling between the positive wave of Ca^{2+} in the cytosol and the negative wave in the ER has several potential implications. First, diffusion and buffering in ER might exert significant effects on wave propagation in the cytosol because the ER is highly buffered, which reduces the effective diffusion of Ca^{2+} in that compartment. Indeed, when we slowed the diffusion of calcium in the ER by decreasing the Ca^{2+} diffusion constant (D_{Ca}^{ER}), the speed of trigger waves was found to decrease. For sufficient decreases, the wave even terminated. Similar results are observed when the fraction of mobile buffer in the ER is decreased below 24%. Varying the fraction of mobile buffer in the ER for suprathreshold wave trains, on the other hand, had a negligible effect on wave propagation. Even eliminating Eq. 4 from the calculations and simply setting $[Ca^{2+}]_{ER}$ to a fixed

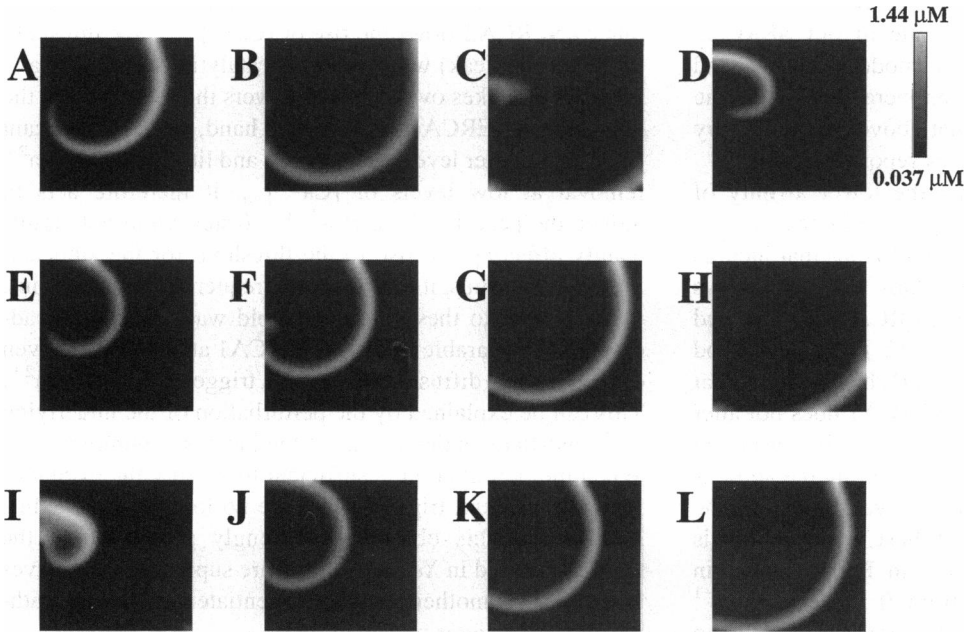

FIGURE 10 Continuation of simulation in Fig. 9. At t = 400 s, the diffusion constants are all set to zero. The center of the spiral does not remain stable. Frame *A* starts at t = 420 s, with 5-s intervals between frames.

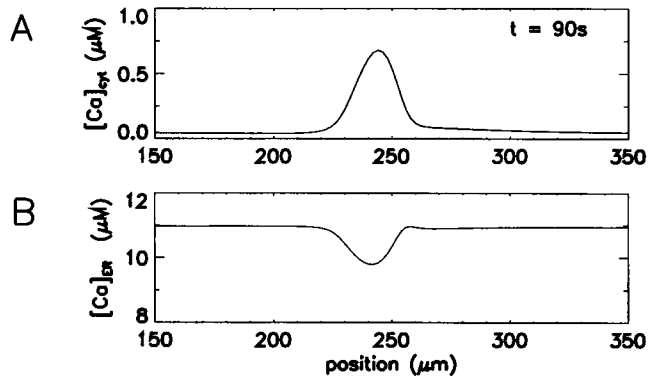

FIGURE 11 (*A*) The Ca^{2+} wave train generated as in Fig. 4. (*B*) The accompanying Ca^{2+} depletion wave in the ER.

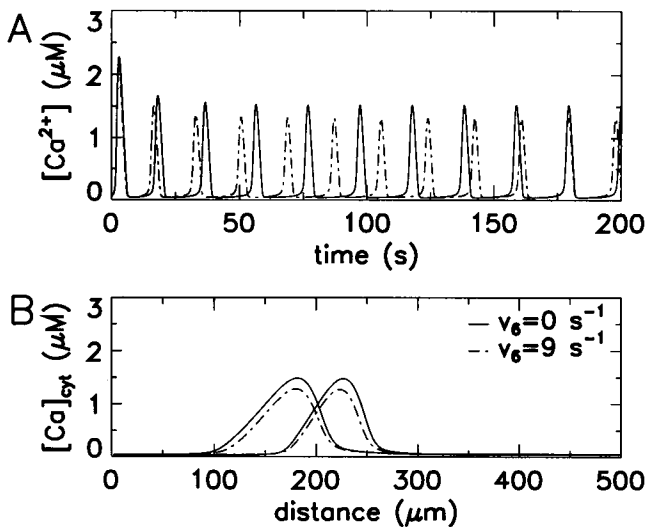

FIGURE 12 The frequency of the oscillations increases as the simulated expression of SERCA1 increases. (*A*) Without SERCA1 (full line; $v_6 = 0$ $\mu M \cdot s^{-1}$) the period is 20.6 s; the period is 18.5 s with SERCA1 (dashed line; $v_6 = 9$ $\mu M \cdot s^{-1}$). (*B*) The wave speed is unchanged when SERCA1 is included in the simulations. Waves initiated by an IP_3 pulse with $[IP_3]^* = 0.52$ μM. Both traces show two waves at $t = 183$ s and at $t = 185$ s.

value in the range 10–15 μM did not appreciably alter the appearance of the wave trains.

Another way to modify Ca^{2+} handling by the ER was developed by Camacho and Lechleiter (1993), who have expressed the SERCA1 Ca^{2+} pump in *Xenopus laevis* oocytes. Their experiments show higher frequency oscillations than in the native oocyte, which contains the SERCA2b isoform. Furthermore, the wave speed in the modified oocyte is unchanged from the native oocyte. They have suggested that the increased rate of pumping shortens the refractory period for Ca^{2+} release by controlling the Ca^{2+}-dependent mechanism of inhibition. The two possible mechanisms of inhibition they suggest are 1) high $[Ca^{2+}]_{cyt}$ inhibiting IP_3R and 2) depletion of the Ca^{2+} stores. Additional pump activity will certainly both lower $[Ca^{2+}]_{cyt}$ and increase $[Ca^{2+}]_{ER}$, contributing to both effects. However, previous calculations, in which simply increasing the removal rate of Ca^{2+} from the cytosol was examined, show that this decreases the frequency of oscillations (Jafri and Gillo, 1994; Sneyd et al., 1993). We confirmed this observation by increasing the maximum rate of our SERCA2 pump, v_3. Using a rather different model (Dupont and Goldbeter, 1994) similar conclusions were reached in the oscillatory range despite the fact that above the oscillatory threshold an increased frequency was reported.

It therefore seemed possible that the lower affinity of SERCA1 for Ca^{2+} might play a role in increasing the frequency, and we have carried out simulations that include an additional term for the SERCA1 pumps. Fig. 12 *A* shows that when v_6, the maximum rate of SERCA1, is increased from 0.0 to 9.0 $\mu M \cdot s^{-1}$ ($[IP_3]^* = 0.52$ μM), the period decreases from 20.6 s to 18.5 s. Fig. 12 *B* shows further that our simulation of the expression of SERCA1 does not alter the wave speed of the Ca^{2+} wave train, which is constant at 22 $\mu m \cdot s^{-1}$. This can be explained by recalling the approximate relationship, $c = \lambda/\tau$, among wave speed (c), the wavelength (λ), and the period (τ) of these waves, which is shown for $v_6 = 0$ and 40 $\mu M \cdot s^{-1}$ in Fig. 7. Note, in particular, when v_6 is increased from 0 to 40 $\mu M \cdot s^{-1}$ ($[IP_3]^* = 0.36$ μM) that the period decreases from 26 to 16.9 s, which is reflected in the increased slope of c versus λ. According to the approximately linear relationship in Fig. 7, if as the period decreases, the wavelength decreases by a similar ratio, then the wave speed will remain unchanged. A smaller wavelength in the presence of SERCA1 expression is clearly evident in the experiments of Camacho and Lechleiter (1993) and supports this explanation. Furthermore, the wave width decreases in the simulated waves, in agreement with the experimental findings.

The difference in the effects of raising the SERCA1 versus the SERCA2 pump rate can be explained by considering the level of $[Ca^{2+}]_{cyt}$ at which each pump is more likely to be active. An increase in the total Ca^{2+} removal rate by SERCA2 slows the rise of $[Ca^{2+}]_{cyt}$ to the threshold (it offsets the leak) where the autocatalytic release of Ca^{2+} from the ER takes over and thus lowers the frequency of the oscillations. SERCA1, on the other hand, has its significant activity at higher levels of $[Ca^{2+}]_{cyt}$ and little effect on Ca^{2+} removal at low levels of $[Ca^{2+}]_{cyt}$. It therefore acts to reduce the peak levels of $[Ca^{2+}]_{cyt}$ faster while not significantly affecting the rise to the threshold for the autocatalytic release. Thus, it increases the frequency of oscillations.

In contrast to these suprathreshold wave properties, addition of comparable fluxes of SERCA1 attenuates and even eliminates the diffusion-dependent trigger waves of Ca^{2+}. This can be explained by the perturbation of the underlying Ca^{2+} oscillations that occurs at the increased pumping rate. When the perturbation is sufficient to destroy the excitability of the system, trigger waves are no longer stable (Murray, 1990). This observation strongly suggests that the waves observed in *Xenopus laevis* are suprathreshold waves and provides another test to differentiate between suprathreshold and trigger waves in vivo.

ROLE OF STATIONARY AND MOBILE BUFFERS

The effects of stationary and mobile buffers on Ca^{2+} waves enter into our equations in three different ways. Referring to Eq. 1, the first term inside the square brackets represents an effective diffusive flux of Ca^{2+} that depends on the concentration of buffers. This gives a Ca^{2+}-dependent effective diffusion constant:

$$D_{\text{eff}} = \beta_{\text{cyt}}(D_{\text{Ca}}^{\text{cyt}} + \gamma_{\text{m}}^{\text{cyt}} D_{\text{m}}^{\text{cyt}} + \gamma_{\text{e}}^{\text{cyt}} D_{\text{e}}^{\text{cyt}}), \qquad (11)$$

where β_{cyt} is the differential fraction of free cytoplasmic Ca^{2+} defined in Eq. 2. Thus for a fixed value of $[Ca^{2+}]_{\text{cyt}}$, the values of the total concentration of stationary (s) and mobile (m) endogenous and exogenous (e) buffers, $[B_i]_{\text{cyt}}$, determine the size of the effective diffusion constant, and, therefore, the size of the diffusive term in the Ca^{2+} balance equation. The second term in Eq. 1 represents a nondiffusive contribution of the rapid mobile buffers due to the uptake of $[Ca^{2+}]_{\text{cyt}}$ as free Ca^{2+} moves down gradients (Wagner and Keizer, 1994). For all values of the gradient its net effect is to lower local Ca^{2+} concentrations. Finally, the factor β_{cyt} multiplies the Ca^{2+} influx and efflux terms from the ER. Because β_{cyt} is considerably less than unity, it reduces the influence of the ER. Recalling its definition in Eq. 2, its value is smaller at lower Ca^{2+} concentrations or higher concentrations of total buffers.

Endogenous buffers

The standard parameters given in Table 3 include only endogenous buffers having a net total concentration of 300 μM and a mobile fraction ($D_{\text{m}} = 75\ \mu\text{m}^2 \cdot \text{s}^{-1}$) of 25%. The effects of altering the net total concentration of buffer on trigger waves and wave trains, with the percentage of mobile buffer maintained at 25%, are shown in Fig. 13, *A* and *B*. There the wave speeds, amplitudes, and half-amplitude wave widths are shown. All three of these quantities are affected by the net total endogenous buffer concentration, with somewhat larger effects on the suprathreshold than the subthreshold waves. Changes in the wave speed and wave amplitude of about a factor of 2 occur over the physiological range of 100–300 μM of endogenous buffer. Because of the low affinity of the mobile buffers used in these calculations, the influence of the nondiffusive term in Eq. 1 is negligible (Wagner and Keizer, 1994). Thus, these changes are due to a combination of changes to the effective diffusion constant and to the extent of Ca^{2+} buffering (β_{cyt}).

To isolate the buffering effects caused by D_{eff} from those cause by β_{cyt}, simulations were performed in which the total endogenous buffer concentration was held fixed while the dissociation constants for the mobile and stationary endogenous buffers were set equal ($K_{\text{m}} = K_{\text{s}} = 8\ \mu$M) and the fraction of mobile buffer was varied. Under these conditions Eq. 2 shows that β_{cyt} remains constant, and Eqs. 3 and 11 show that D_{eff} increases as the percentage mobile buffer changes from 0 to 100%. Results are summarized in Fig. 14, where now the results for wave trains (*A*) and trigger waves (*B*) are seen to be quite different. In agreement with our earlier observations about the lack of influence of diffusion on waves in the oscillatory regime, the increase in D_{eff} has a negligible effect on the properties of repetitive wave trains. For the diffusion-dependent trigger waves, on the other hand, there is no wave propagation at low fractions of mobile buffer. This cannot be attributed to an alteration in the underlying properties of the ER Ca^{2+} oscillator, because they do not change (Wagner and Keizer, 1994) as the form of β_{cyt} is fixed in these simulations. Thus, the dramatic changes due to mobile buffers must be due to the diffusive term in Eq. 1.

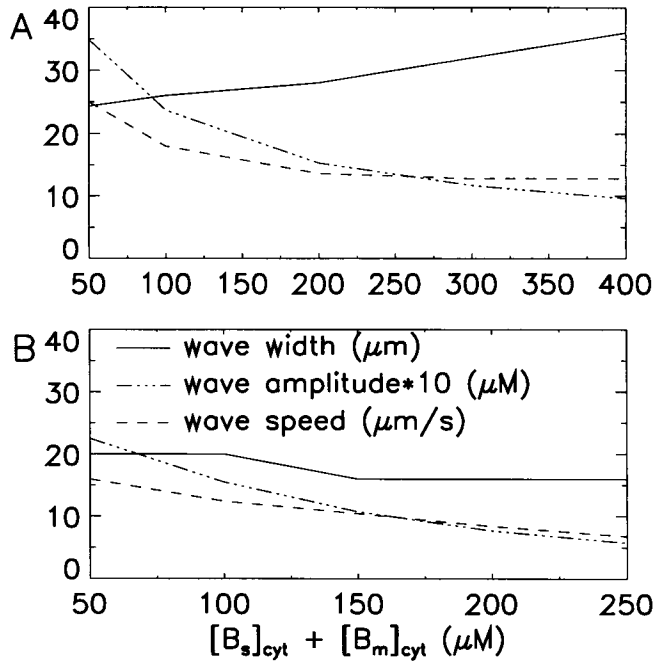

FIGURE 13 The wave speed and amplitude decrease with increasing endogenous buffer concentration for both (*A*) suprathreshold waves ($[IP_3]^* = 0.36\ \mu$M) and (*B*) subthreshold waves ($[IP_3]^* = 0.245\ \mu$M). The wave width remains relatively constant for trigger waves (*B*), whereas the wave width increases for wave trains (*A*). The fraction of mobile buffer is held constant at 0.25. Data gathered as described in Table 4. Trigger waves were initiated by a 30-μm-wide, 0.4 μM Ca^{2+} pulse starting at $x = 0\ \mu$m.

Using the data in Fig. 14 *B*, we have been able to correlate the wave speed of the trigger waves with D_{eff}. According to earlier work, the effective diffusion constant varies linearly with the mobile buffer concentration (Wagner and Keizer, 1994). Because for the values of $K_{\text{m}} = K_{\text{s}} = 8\ \mu$M used in the simulations, D_{eff} is relatively insensitive to the values of $[Ca^{2+}]_{\text{cyt}}$, and for each concentration of mobile buffer in Fig. 14 *B* we calculated the value of D_{eff} at $[Ca^{2+}]_{\text{cyt}} = 0.1\ \mu$M. Fig. 14 *C* then shows the square of the wave speed plotted versus these values of D_{eff}. The excellent linear correlation expresses the fact that for trigger waves

$$c^2 = (D_{\text{eff}}/\tau_1)^{-a}, \qquad (12)$$

where $1/\tau_1$ is the slope in Fig. 14 *C* ($\approx 1\ \text{s}^{-1}$) and a is the intercept. This is reminiscent of the so-called Luther equa-

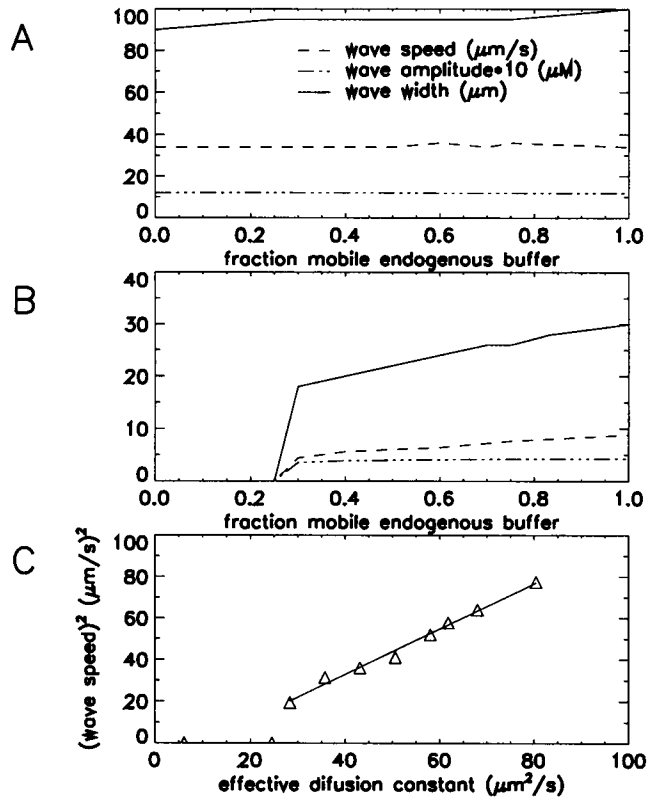

FIGURE 14 Upper two panels show wave speed, amplitude, and width for a constant total concentration of endogenous buffers (300 μM, $K_m^{cyt} = K_s^{cyt} = 8$ μM) as a function of the fraction of buffer that is mobile. (*A*) suprathreshold wave trains generated as in Fig. 3 with $[IP_3]^* = 0.36$ μM. (*B*) subthreshold waves generated as in Fig. 5 with $[IP_3]^* = 0.245$ μM. (*C*) Square of trigger wave speed in (*B*) plotted versus D_{eff} (see text for details). Slope of the straight line is 1.1 s^{-1}.

tion, in which τ_1 is interpreted as being on the order of the rise time for the wave front (Jaffe, 1993). Indeed, the rise time in Fig. 12 *A* is on the order of 1–2 s. It is worth reiterating, however, that this result does not hold for suprathreshold wave trains, which Fig. 14 *A* shows are insensitive to changes in the effective diffusion constant.

Exogenous buffers and indicators

A variety of exogenous Ca^{2+} buffers have been used to investigate the properties of Ca^{2+} handling in cells. Indeed, fluorescent Ca^{2+} dyes, such as fura-2, fluo-3, and calcium green, which are used to image Ca^{2+} waves, are high-affinity buffers of Ca^{2+}. Although there is little experimental information on the effects of these exogenous buffers on either Ca^{2+} oscillations or waves, high concentrations of fura-2 are known to alter the speed of the fertilization Ca^{2+} wave in *Xenopus laevis* oocytes (Nuccitelli et al., 1993). Although these changes may be due to the effect of fura-2 on the IP_3R (Richardson and Taylor, 1993), they may also result from the buffering power of fura-2.

We have carried out simulations of planar Ca^{2+} waves with varying concentrations and affinities of exogenous buffers. The effect on the waves is summarized in Table 4. For simplicity, we have assumed that the diffusion constant for each buffer is $D_e^{cyt} = 75$ $\mu m^2 \cdot s^{-1}$. The buffers differ in their affinities, with K_Ds of 0.16, 0.2, and 1.5 μM chosen to approximate fura-2, calcium green, and dibromo-BAPTA. All simulations were carried out in the oscillatory regime. Note that the amplitude of the waves decreases as the concentration of each buffer increases from 0 to 80 μM. This can be attributed in part to the decrease in β_{cyt}, which has been calculated at the half-amplitude of the wave and included in Table 4, and in part to the increase in the nondiffusive term, which is greater for the high-affinity buffers.

Table 4 shows that the effective diffusion constant of Ca^{2+}, D_{eff}, increases by less than roughly 20% for the high-affinity buffers fura-2 and calcium green and roughly 40% for dibromo-BAPTA as the buffer concentration increases. However, as shown in Fig. 14 *A*, changes in D_{eff} have little effect on the properties of these waves and thus play only a minor role in the changes in Table 4. The small changes in the wave speed for all of the buffers show a slight increase at intermediate concentrations followed by decreases at higher concentrations. This can also be explained by the combined effect of the exogenous buffers on the nondiffusive term in Eq. 1, which causes an increase in the wave speed, and on the ER handling terms (β_{cyt}), which cause a decrease.

The buffers have a striking effect on the wave width, which increases by about a factor of 2 in the fura-2 simulations. This is illustrated further in Fig. 15, which compares the wave shape of the Ca^{2+} wave at the five concentrations of fura-2 shown in Table 4. Because simply decreasing the amplitude of the underlying Ca^{2+} oscillations does not increase the wave width appreciably, this effect must be due predominately to the nondiffusive term in Eq. 1. That term represents the sequestering of Ca^{2+} by mobile buffers as free Ca^{2+} moves down its gradient. The larger the gradient and the higher the concentration of the mobile buffers, the larger is the effect of the nondiffusive term in lowering the gradient and increasing the width of the waves in Fig. 15.

Ca^{2+} indicators can be combined with macromolecules like dextran to yield significantly less mobile buffer (Girard and Clapham, 1993). Table 5 shows the results of calculations used to simulate the effect on planar Ca^{2+} waves of a variety of mixtures of fura-2 ($D_e^{cyt} = 75$ $\mu m^2 \cdot s^{-1}$) and fura-2 dextran with its substantially reduced mobility (taken for simplicity as $D_e^{cyt} = 0$ $\mu m^2 \cdot s^{-1}$). The small decrease of the amplitude as the percentage mobile fura-2 increases for a fixed total concentration of buffer is due to the nondiffusive term because β_{cyt}, and therefore the diffusive term, does not change in those calculations. The increase in the wave width as the percentage mobile fura-2 increases is explained, as in Table 4, by the influence of the mobile buffers on the nondiffusive term in the calcium balance Eq 1. The wave speed is also an increasing function of the mobility of the buffer for a fixed total concentration. Because the change in mobility does not affect ER Ca^{2+}

TABLE 4 The effects of Ca^{2+} dyes on Ca^{2+} waves

	Amplitude (μM)	Width (μm)	Speed ($\mu m \cdot s^{-1}$)	β_{cyt}	D_{eff} ($\mu m^2 \cdot s^{-1}$)
Fura-2	K_D = 0.16 μM				
[Fura-2] (μM)					
0	1.19	34	14.4	0.06	32.7
10	1.09	44	14.4	0.05	32.7
20	1.02	42	16.8	0.05	32.9
40	0.84	44	15.2	0.05	33.6
80	0.51	72	14.8	0.03	37.7
Dibromo-BAPTA	K_D = 1.5 μM				
[Dibromo-BAPTA] (μM)					
0	1.19	34	14.4	0.06	32.7
10	1.09	36	14.0	0.05	33.8
20	1.02	40	14.8	0.05	35.1
40	0.88	44	14.0	0.04	38.1
80	0.68	48	12.8	0.03	44.3
[Calcium green]	K_D = 0.2 μM				
[Calcium green] (μM)					
0	1.19	34	14.4	0.06	32.7
10	1.08	36	14.0	0.05	32.8
20	0.99	40	15.2	0.05	33.0
40	0.79	40	13.2	0.04	34.0
80	0.46	54	11.2	0.03	39.6

The addition of mobile fluorescent dyes results in an increase in wave speed and width and a decrease in amplitude. Notice that the lower the K_D the greater the increase in the wave width and the less the change in the effective diffusion constant. The effects on waves with increasing buffer concentration are the result of the interaction between the decrease in the factor β_{cyt} and the increase in the effective diffusion constant D_{eff}. Data were obtained from waves generated by an initial ramp of $[IP_3]$ 2.75 μM at the left boundary and 0.25 μM at the right boundary. Speeds were obtained by measuring the positions of a wave at two times 5 s apart. The amplitude and width values were taken from the wave at end of the 5-s interval. The width is the values measured at half-amplitude. ($[IP_3]^*$ = 0.36 μM).

handling through β_{cyt} and because diffusive effects are small, we conclude that these increases in speed are due solely to the nondiffusive effects of the mobile buffer.

CONCLUDING REMARKS

By carrying out simulations with a model of IP_3-induced Ca^{2+} oscillations that includes the effects of Ca^{2+} buffering, Ca^{2+} diffusion, and Ca^{2+} handling by the ER, we have attempted to sort out the relative contributions of each of these features to traveling waves of Ca^{2+}. Perhaps the most striking conclusion is that although Ca^{2+} diffusion plays an essential role for trigger waves that occur in the excitable regime (just below the oscillation threshold), it plays only a secondary role for repetitive wave phenomena that occur in the oscillatory regime. For trigger waves, we find a linear correlation between the square of the speed of wave propagation and an effective diffusion constant for Ca^{2+}, whose reduced value is determined by the stationary and mobile buffers. The characteristics of repetitive waves, including planar wave trains and target patterns and spiral waves in two dimensions, suggest an important role for the rapid, unbuffered diffusion of IP_3. In our calculations the patterns of wave activity in the oscillatory regime are dominated by the relative phases of the oscillatory uptake and release of Ca^{2+} occurring in local regions, so that they are not strongly dependent on Ca^{2+} diffusion. By coordinating the phases of adjacent regions, the diffusion of IP_3 can organize the cytoplasm into traveling waves. We find that the buffered diffusion of Ca^{2+} contributes primarily to the shape of these waves and, in the case of two-dimensional spiral waves, to the maintenance of the organizing center.

As the compartment that controls the release of intracellular Ca^{2+}, the ER plays an important role in both the initiation and propagation of Ca^{2+} waves. The dynamic feedback of $[Ca^{2+}]_{cyt}$ on the IP_3R combined with the reuptake of Ca^{2+} by

TABLE 5 The effects of fura/fura-dextran on Ca^{2+} waves

[Fura-2] (μM)	% mobile	Amplitude (μM)	Width (μm)	Speed ($\mu m \cdot s^{-1}$)
0	—	1.19	34	14.4
10	100	1.09	36	14.4
10	75	1.09	34	13.8
10	50	1.09	34	12.8
10	25	1.09	32	12.8
10	0	1.09	30	12.0
80	100	0.51	72	14.8
80	75	0.51	54	12.4
80	50	0.51	46	10.4
80	25	0.53	34	8.8
80	0	0.55	38	8.0

An increase in the mobility of the exogenous buffer causes an increase in the wave speed and width. The effect is more pronounced at higher buffer concentrations. A slight decrease in wave amplitude is seen with increasing mobility at high buffer concentrations. The data were gathered as described in Table 4.

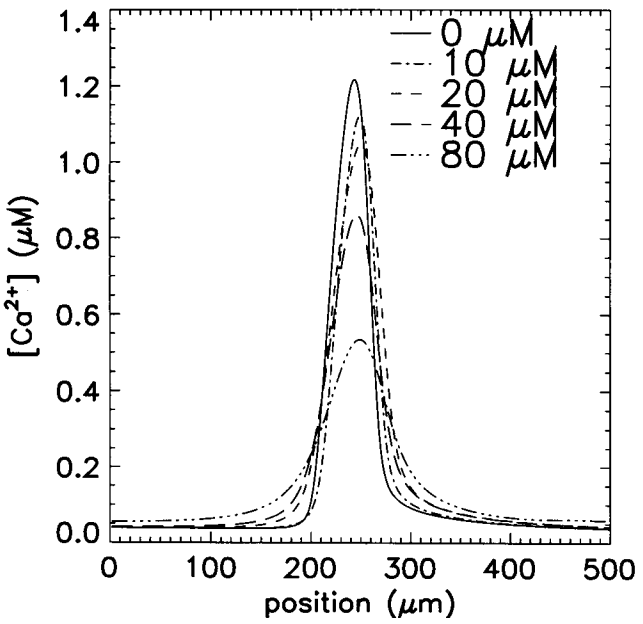

FIGURE 15 Wave profiles for the five simulated fura-2 concentrations in Table 4. As the concentration of fura-2 increases, the width of the wave increases while the amplitude decreases.

the SERCA pumps determines the threshold level at which IP_3 can generate Ca^{2+} waves. Indeed, in our calculations the addition of a SERCA1-type pump increases the frequency of the oscillations. In agreement with recent experiments (Camacho and Lechleiter, 1993), we find that this does not change the wave speed and conclude that it is the lower affinity of the pump for Ca^{2+} that leads to these results. The fact that the SERCA1 pump eliminates trigger waves suggests that in *Xenopus laevis* oocytes the waves occur in the oscillatory regime. This is also suggested by the fact that the range of $[IP_3]$ that supports oscillations is roughly an order of magnitude larger than that which supports excitability. Because of the difference in size of the cytosolic and ER compartments (volume ratio $\approx$ 5/1), we find that a significant depletion wave of ER Ca^{2+} accompanies the passage of a cytosolic Ca^{2+} wave. This is reminiscent of the depletion wave observed in isolated cortices from sea urchin eggs (Terasaki and Sardet, 1991), and we find depletion waves in both the excitable and oscillatory regimes. They may play an important part in Ca^{2+} signal transduction, especially for cells in which lumenal Ca^{2+} helps regulate ER Ca^{2+} release (Missiaen *et al.*, 1992).

The role that Ca^{2+} buffers play in Ca^{2+} waves is closely related to both Ca^{2+} diffusion and Ca^{2+} uptake and release from the ER. Based on our assumption that buffering occurs rapidly with respect to Ca^{2+} diffusion (Wagner and Keizer, 1994), buffers give rise to 1) a substantially reduced effective diffusion constant for Ca^{2+} (D_{eff}), 2) a nondiffusive transport of Ca^{2+} caused by the uptake of Ca^{2+} by mobile buffers, and 3) an alteration of Ca^{2+} uptake and release through the differential fraction of free Ca^{2+} (β_{cyt}). The first of these is responsible for the slow diffusive transport of Ca^{2+} that is key in determining the speed of trigger waves and the properties of the organizing center of spiral waves. The nondiffusive effect of mobile buffers is most important when their affinity is high, as it is for commonly used Ca^{2+} indicators. Analysis of our simulations shows that elevated concentrations of indicators like fura-2 or calcium green can significantly decrease the amplitude and increase the width of Ca^{2+} waves. The decrease in amplitude is due primarily to the decrease in the fraction of free Ca^{2+}, whereas the increase in wave width is due to the nondiffusive effects when the indicators are mobile. Although conjugating the indicator to a less mobile species like dextran will eliminate the nondiffusive effect, the fraction of free Ca^{2+} is not altered, and so the amplitude and speed of the wave remain reduced.

We would like to thank Greg Smith and John Wagner for helpful discussions.

This work was supported by NSF grants BIR 9300799 and BIR 9214381 and the UC Agricultural Experiment Station.

REFERENCES

Allbritton, N. L., T. Meyer, and L. Stryer. 1992. Range of messenger action of calcium ion and inositol 1,4,5-triphosphate. *Science.* 258:1812–1815.

Ames, W. F. 1977. Numerical Methods for Partial Differential Equations, 2nd ed. Academic Press, New York.

Atri, A., J. Amundson, D. Clapham, and J. Sneyd. 1993. A single-pool model for intracellular calcium oscillations and waves in the *Xenopus laevis* oocyte. *Biophys. J.* 65:1727–1739.

Berridge, M. J. 1993. Inositol trisphosphate and calcium signalling. *Nature.* 361:315–325.

Bezprozvanny, I., J. Watras, and B. E. Ehrlich. 1991. Bell-shaped calcium response curves of $Ins(1,4,5)P_3$- and calcium-gated channels from endoplasmic reticulum of cerebellum. *Nature.* 351:751–754.

Camacho, P., and J. D. Lechleiter. 1993. Increased frequency of calcium waves in *Xenopus laevis* oocytes that express a calcium-ATPase. *Science.* 260:226–229.

De Young, G., and J. Keizer. 1992. A single-pool inositol 1,4,5,-trisphosphate-receptor-based model for agonist-stimulated oscillations in Ca^{2+} concentration. *Proc. Natl. Acad. Sci. USA.* 89:9895–9899.

Dupont, G., and A. Goldbeter. 1992. Oscillations and waves of cytosolic calcium—insights from theoretical models. *Bioessays.* 14:485–493.

Dupont, G., and A. Goldbeter. 1994. Properties of intracellular Ca^{2+} waves generated by a model based on Ca^{2+}-induced Ca^{2+} release. *Biophys. J.* 67:2191–2204.

Finch, E. A., T. J. Turner, and S. M. Goldin. 1991. Calcium as a coagonist of inositol 1,4,5,-trisphosphate induced calcium release. *Science.* 252: 443–446.

Girard, S., and D. Clapham. 1993. Acceleration of intracellular calcium waves in *Xenopus* oocytes by calcium influx. *Science.* 260:229–232.

Girard, S., A. Luckhoff, J. Lechleiter, J. Sneyd, and D. Clapham. 1992. Two-dimensional model of calcium waves reproduces the patterns observed in *Xenopus* oocytes. *Biophys. J.* 61:509–517.

Jaffe, L. 1993. Classes and mechanisms of calcium waves. *Cell Calcium.* 14:736–745.

Jafri, M. S. 1995. A theoretical study of cytosolic calcium waves. *J. Theor. Biol.* 172:209–216.

Jafri, M. S., and B. Gillo. 1994. A membrane potential model with counterions for cystosolic calcium oscillations. *Cell Calcium.* 16:9–19.

Jafri, M. S., and J. Keizer. 1994. Diffusion of inositol 1,4,5,-trisphosphate but not Ca^{2+} is necessary for a class of inositol 1,4,5,-trisphosphate-induced Ca^{2+} waves. *Proc. Natl. Acad. Sci. USA.* 91:9485–9489.

Jafri, M. S., S. Vajda, P. Pasik, and B. Gillo. 1992. A membrane model for cytosolic calcium oscillations: a study using *Xenopus* oocytes. *Biophys. J.* 63:235–246.

Keener, J. P., and J. J. Tyson. 1986. Spiral waves in the Belousov-Zhabotinskii reaction. *Physica D.* 21:307–324.

Keizer, J., and G. W. De Young. 1992. Two roles for Ca^{2+} in agonist stimulated Ca^{2+} oscillations. *Biophys. J.* 61:649–660.

Keizer, J., and G. De Young. 1994. Simplification of a realistic model of $[IP_3]$-induced Ca^{2+} oscillations. *J. Theor. Biol.* 166:431–442.

Kopell, N., and L. N. Howard. 1973. Horizontal bands in the Belousov reaction. *Science.* 180:1171–1173.

Lapidus, L., and G. F. Pinder. 1982. Numerical Solution of Partial Differential Equations in Science and Engineering, 1st ed. Wiley, New York.

Lechleiter, J. D., and D. E. Clapham. 1992. Molecular mechanisms of intracellular calcium excitability in *X. laevis* oocytes. *Cell.* 69:283–294.

Lechleiter, J., S. Girard, E. Peralta, and D. Clapham. 1991. Spiral calcium wave propagation and annihilation in *Xenopus laevis* oocytes. *Science.* 252:123–126.

Li, Y. X., J. Rinzel, J. Keizer, and S. S. Stojilkovic. 1994. Calcium oscillations in pituitary gonadotrophs—comparison of experiment and theory. *Proc. Natl. Acad. Sci. USA.* 91:58–62.

Lytton, J., M. Westlin, S. E. Burk, G. E. Shull, and D. H. MacLennan. 1992. Functional comparisons between isoforms of the sarcoplasmic or endoplasmic reticulum family of calcium pumps. *J. Biol. Chem.* 267: 14483–14489.

Milner, R. E., K. S. Famulski, and M. Michalak. 1992. Calcium binding proteins in the sarcoplasmic/endoplasmic reticulum of muscle and non-muscle cells. *Mol. Cell. Biochem.* 112:1–13.

Missiaen, L., H. Desmedt, G. Droogmans, and R. Casteels. 1992. Luminal Ca^{2+} controls the activation of the inositol 1,4,5-trisphosphate receptor by cytosolic Ca^{2+}. *J. Biol. Chem.* 267:22961–22966.

Miyazaki, S., M. Yuzaki, K. Nakada, H. Shirakawa, S. Nakanishi, S. Nakade, and K. Mikoshiba. 1992. Block of Ca^{2+} wave and Ca^{2+} oscillation by antibody to the inositol 1,4,5-trisphosphate receptor in fertilized hamster eggs. *Science.* 257:251–255.

Murray, J. D. 1990. *Mathematical Biology.* Springer-Verlag, New York.

Neher, E., and G. J. Augustine. 1992. Calcium gradients and buffers in bovine chromaffin cells. *J. Physiol. (Lond.).* 450:273–301.

Nuccitelli, R., D. L. Yim, and T. Smart. 1993. The sperm-induced Ca^{2+} wave following fertilization of the *Xenopus* egg requires the production of $Ins(1,4,5)P_3$. *Dev. Biol.* 158:200–212.

Parys, J. B., S. M. McPherson, K. P. Campbell, and F. J. Longo. 1994. Presence of inositol 1,4,5-trisphosphate receptor, calreticulin, and calsequestrin in eggs of sea urchin and *Xenopus laevis*. *Dev. Biol.* 161: 466–476.

Richardson, A., and C. W. Taylor. 1993. Effects of Ca^{2+} chelators on purified inositol 1,4,5-trisphosphate ($InsP_3$) receptors and $InsP_3$-stimulated Ca^{2+} mobilization. *J. Biol. Chem.* 268:11528–11533.

Rooney, T. A., and A. P. Thomas. 1993. Intracellular calcium waves generated by $Ins(1,4,5)P_3$-dependent mechanisms. *Cell Calcium.* 14: 674–690.

Ross, J., S. C. Mueller, and C. Vidal. 1988. Chemical waves. *Science.* 240:460–465.

Sneyd, J., and A. Atri. 1993. Curvature dependence of a model for calcium wave propagation. *Physica D.* 65:365–372.

Sneyd, J., B. T. R. Wetton, C. Charles, and M. J. Sanderson. 1995. Calcium waves mediated by diffusion of inositol trisphosphate: a two dimensional model. *Am. J. Physiol.* 268:C1537–C1545.

Sneyd, J., S. Girard, and D. Clapham. 1993. Calcium wave propagation by calcium-induced calcium release—an unusual excitable system. *Bull. Math. Biol.* 55:315–344.

Somlyo, A. P., M. Bond, and A. V. Somlyo. 1985. Calcium content of mitochondria and endoplasmic reticulum in liver frozen rapidly in vivo. *Nature.* 314:622–625.

Terasaki, M., and C. Sardet. 1991. Demonstration of calcium uptake and release by sea urchin egg cortical endoplasmic reticulum. *J. Cell Biol.* 115:1031–1037.

Tse, A., F. W. Tse, and B. Hille. 1994. Calcium homeostasis in identified rat gonadotrophs. *J. Physiol. (Lond.).* 477:511–525.

Wagner, J., and J. Keizer. 1994. Effects of rapid buffers on Ca^{2+} diffusion and Ca^{2+} oscillations. *Biophys. J.* 67:447–456.

Zhou, Z. A., and E. Neher. 1993. Mobile and immobile calcium buffers in bovine adrenal chromaffin cells. *J. Physiol. (Lond.).* 469:245–273.